Nuclear Instruments and Methods in Physics Research A 1092 (2026) 171898

Contents lists available at ScienceDirect

Nuclear Inst. and Methods in Physics Research, A

journal homepage: www.elsevier.com/locate/nima

Full Length Article

Experimental evaluation of a SPECT module for prompt gamma-based dose monitoring in Boron Neutron Capture Therapy[☆]

F. Ghisio [a,b,*], T. Ferri [a,b], M. Pandocchi [a,b], M. Carminati [a,b], C. Fiorini [a,b], G. Mocerino [c,b], L. Grisoni [c,b], D. Mazzucconi [c,b], D. Ramos [d,e], G. Iaselli [d,e], G. Pugliese [d,e], V. Pascali [f,g], N. Protti [f,g], G. Borghi [a,b,**]

[a] Dipartimento di Elettronica, Informazione e Bioingegneria, Politecnico di Milano, 20133 Milan, Italy
[b] Istituto Nazionale di Fisica Nucleare, Sezione di Milano, 20133 Milan, Italy
[c] Dipartimento di Energia, Politecnico di Milano, 20133 Milan, Italy
[d] Dipartimento di Fisica, Politecnico di Bari, 70126 Bari, Italy
[e] Istituto Nazionale di Fisica Nucleare, Sezione di Bari, 70125 Bari, Italy
[f] Dipartimento di Fisica, Università di Pavia, 27100 Pavia, Italy
[g] Istituto Nazionale di Fisica Nucleare, Sezione di Pavia, 27100 Pavia, Italy

ARTICLE INFO

Keywords:
Boron Neutron Capture Therapy
Dose monitoring
Gamma detector
Shielding
Spect detection module

ABSTRACT

Boron Neutron Capture Therapy (BNCT) is an advanced cancer treatment that combines radiation therapy with targeted drug delivery. It is promising for treating tumors that are challenging to address with conventional methods, but requires precise dose monitoring to work effectively. This can be achieved by detecting the prompt 478 keV gamma rays produced by boron neutron capture reactions during irradiations. In this work, we present experimental measurements performed with a single-unit SPECT module based on a new version of the BeNEdiCTE detector. The detector uses a $LaBr_3$(Ce, Sr) monolithic crystal read out by silicon photomultipliers and custom electronics. To minimize background contribution, the new version of the BeNEdiCTE detector features electronic boards realized with a boron-free material and a new case in Teflon. It also features reduced dead time, enabling reliable operation under high neutron flux conditions. We analyzed background and evaluated the impact of various detector materials and shielding configurations at the Laboratorio di Energia Nucleare Applicata (LENA) in Pavia, Italy. We detected boron concentrations down to 250 ppm in a volume of 5 mL during measurements with a neutron flux of $3.14 \times 10^6\ \mathrm{n\,cm^{-2}\,s^{-1}}$. We also performed tomographic measurements by rotating the SPECT module at four different angles around the sample. We successfully detected the boron signal at all angles and reconstructed a 3D image of a couple of vials with a spatial resolution better than 1 cm. These results demonstrate the potential of the BeNEdiCTE detector for real-time monitoring of boron distribution during BNCT.

1. Introduction

Cancer is one of the leading causes of death globally, accounting for nearly 10 million deaths in 2022 [1]. In recent years, alongside traditional treatments like surgery and chemotherapy, a variety of techniques using ionizing radiation and charged particles have been developed for cancer therapy. Among these, hadron therapy uses protons and carbon ions to precisely deliver high doses of radiation to the tumor while minimizing damage to the surrounding healthy tissue [2]. Although effective for well-defined tumors, hadron therapy encounters challenges when treating diffuse or infiltrative cancers, particularly those located near vital structures or those with irregular shapes [3]. In this context, Boron Neutron Capture Therapy (BNCT) has emerged as a promising and highly personalized treatment option [4].

BNCT is an advanced cancer treatment that provides the unique benefit of targeting tumor cells at the cellular level. This therapy utilizes the interaction between a non-radioactive boron-10 (^{10}B) compound and low-energy thermal neutrons. After the ^{10}B compound is introduced into the patient, it selectively binds to tumor cells. The patient is then

☆ This work was supported in part by INFN Gruppo V, Italy (SPOC project) and in part by the PRIN PNRR 2022 Funding Program of Ministero Dell'Università e della Ricerca (MUR), Italy (BNCT-SPECT Project).
* Corresponding author at: Dipartimento di Elettronica, Informazione e Bioingegneria, Politecnico di Milano, 20133 Milan, Italy.
** Corresponding author.
E-mail addresses: filippo.ghisio@polimi.it (F. Ghisio), giacomo.borghi@polimi.it (G. Borghi).

https://doi.org/10.1016/j.nima.2026.171898
Received 5 March 2026; Received in revised form 1 July 2026; Accepted 19 July 2026
Available online 27 July 2026
0168-9002/

irradiated with a neutron beam, and the ^{10}B atoms capture the neutrons initiating the ^{10}B(n, α)^{7}Li reaction. This reaction produces an alpha particle and a lithium nucleus, both of which are high-LET particles that travel only short distances, comparable to the diameter of a single cell. As a result, the radiation's destructive effects are mainly affecting the boron-enriched tumor cells, while the surrounding healthy tissue receives a significantly lower dose [5].

Although the idea of BNCT originated in the 1930s, clinical trials did not begin until the late 20th century [6,7]. The early development of BNCT faced many challenges, mainly because it relied on nuclear reactors to produce the high-intensity neutron beams needed for treatment. This created significant logistical and safety issues, making it difficult to use in medical settings. However, recent advancements in accelerator technology have renewed interest in BNCT, allowing for the creation of treatment units that are now compatible with hospitals [8]. As a result, the number of BNCT facilities worldwide is growing, with 33 currently operational or under construction, according to the International Society for Neutron Capture Therapy [9]. This rapid expansion highlights the urgent need to further advance BNCT technologies to fully integrate them into clinical practice.

As BNCT moves closer to routine clinical adoption, the absence of a real-time dose monitoring technique remains one of its most critical limitations. Current clinical practice relies on Positron Emission Tomography (PET) scans with dedicated tracers, which are performed days or weeks before treatment, and on blood sampling during irradiation. This requires substantial extrapolation to estimate the actual dose delivered to the tumor and surrounding tissues [10]. This approach cannot capture rapid physiological changes or spatial variations in boron uptake, leading to uncertainties in treatment accuracy. Developing a real-time, high-resolution dosimetry system is therefore essential to verify precise dose delivery, improve patient safety, and fully unlock the therapeutic potential of BNCT.

To address this need, a particularly promising non-invasive approach is the detection and imaging of the 478 keV prompt gamma rays emitted in 94% of the ^{10}B(n, α)^{7}Li reactions, which escape the patient's body and can be measured in real time. Because the emission rate of these photons is directly linked to the neutron-capture reaction rate, a dedicated imaging system measuring this signal could provide continuous feedback on boron distribution and the delivered dose during therapy. To perform this task, several state-of-the-art BNCT monitoring concepts have been proposed, including Compton cameras [11–13] and SPECT-based systems [14–18]. However, the intense radiation background generated by competing neutron interactions presents significant technical challenges, highlighting the need for optimized detector designs and reconstruction methods.

Compton cameras are currently attracting significant interest due to their higher intrinsic detection efficiency and their potential capability to discriminate part of the background through kinematic event reconstruction. However, in many Compton-camera implementations, high spatial resolution is obtained by reducing the distance between the detector and the target volume. In BNCT environments, this results in extremely high event rates due to the intense gamma and neutron background, placing stringent requirements on the detector readout and data-processing electronics. Furthermore, imaging performance in BNCT depends not only on detection efficiency, but also on reconstruction stability and operational complexity. Unlike Compton cameras, pinhole SPECT systems rely on direct geometrical collimation rather than kinematic reconstruction, providing a straightforward relation between detected photons and their direction of origin. Therefore, despite the lower intrinsic efficiency associated with mechanical collimation, SPECT-based systems remain attractive when robust operation, high-rate capability, and straightforward image reconstruction are prioritized.

In this work, we propose a scintillator-based gamma-ray detector combined with a pinhole collimator, designed as a single module of a tomographic BNCT-SPECT system composed of multiple units [19]. With respect to previous developed prototypes, we produced a new collimator to increase the module sensitivity and to shorten the distances between sample, collimator, and detector, thus creating a more compact module. We also improved the materials constituting the electronic boards and the mechanical case, in order to reduce neutron interactions with them and thus background contributions. This helps improving the sensibility of the detector with respect to the high expected background during irradiation. Finally, we upgraded the readout electronics to improve the count-rate capability of the detector, making it able to operate reliably under higher neutron fluxes.

In the following sections, we detail the detector design and outline the key improvements introduced in this work, aiming to enhance its performance towards clinical use. Then, we present measurements carried out at an experimental facility equipped with a neutron beam, followed by a comprehensive analysis of the acquired data and the detector's performance.

2. Materials and methods

The experimental measurements were carried out using a single-unit SPECT module. The SPECT module consists of a new version of the BeNEdiCTE gamma-ray detector and a new custom-designed pinhole collimator made of lead. Additionally, a multi-material shielding was used to minimize background interference.

2.1. The BeNEdiCTE detector

The gamma-ray detector, called BeNEdiCTE, is based on a monolithic lanthanum bromide scintillator crystal co-doped with cerium and strontium (i.e., $LaBr_3$:(Ce+Sr)). The crystal was produced by Saint Gobain and measures 5 cm × 5 cm × 2 cm. The light emitted by the crystal is collected by an 8 × 8 matrix of Near Ultraviolet High-Density (NUV-HD) silicon photomultipliers (SiPMs), produced by Fondazione Bruno Kessler (FBK), Trento, Italy [20]. Each of the 64 SiPMs measures about 6 mm × 6 mm and has a cell size of 30 μm × 30 μm. The 64 SiPMs are grouped into 4 tiles, each containing 16 SiPMs in a 4 × 4 matrix configuration. Each tile is equipped with a temperature sensor that continuously monitors the SiPMs temperature. This measurement is used by the electronics to actively regulate the bias voltage in real time, compensating for SiPM gain variations induced by thermal fluctuations.

The signal from the SiPMs is read out by custom electronics. The electronic front-end is based on GAMMA (Gain Amplitude Modulation Multichannel ASIC), an ASIC developed at Politecnico di Milano [21]. Our system comprises four 16-channel GAMMA ASICs. The ASIC receives the current from the SiPMs and routes it toward three different processing paths. One path is dedicated to energy measurement, using a gated integrator with selectable gain, another is used for trigger generation, and the third provides as output the sum of the currents from all 16 SiPMs.

The output of the energy path is digitized externally by four analog-to-digital converters (ADCs), one per ASIC, only if the event is considered valid according to an energy discrimination circuit. The energy discrimination circuit processes the current sum obtained further summing the four current sum signals from the GAMMA ASICs. It aims to perform real-time discrimination of events based on their energy [22]. This circuit comprises a trans-impedance amplifier (TIA), which converts the current into a voltage that is proportional to the energy of the incoming events. This voltage is then compared with two selectable thresholds to define an energy range. Events with energies within this range are processed and recorded, while those outside the range are discarded. A field-programmable gate array (FPGA) handles energy discrimination, data acquisition, and communication with the PC, transferring the acquired data.

The BeNEdiCTE detector achieves an energy resolution better than 3% at 662 keV [18]. The energy resolution at 478 keV is almost equal to 4%, enabling the isolation of the 478 keV peak of interest from the adjacent photopeak at 511 keV of annihilation photons. Additionally, the crystal's 2 cm thickness ensures a good detection efficiency of approximately 60% at 478 keV.

2.2. BeNEdiCTE's dead time

The dead time of a detector is the minimum time interval that must separate two events for them to be recorded as distinct pulses. In the BeNEdiCTE detector, the dead time is mainly determined by two factors: the integration time of the ASICs and the read time of the ADCs. The integration time is the duration required by the ASICs to integrate the current pulses generated by the SiPMs. The read time is the time needed by the ADCs to convert an event. In the BeNEdiCTE module, each ADC reads out 16 channels, with their energy values multiplexed internally by the ASICs and transmitted serially. Therefore, the minimum read time is the time required for a single ADC to perform one conversion, multiplied by the number of channels it processes (i.e., 16).

The dead time is a critical parameter for the BeNEdiCTE detector, as it limits its count rate capability. High counting rates increase the likelihood of dead time losses, leading to missed events that can affect measurement accuracy. To address this, we reduced the dead time from 5.4 μs to 2.1 μs by optimizing the integration time and reducing the read time thanks to faster ADCs [23]. Specifically, we replaced the previous ADCs, which were limited to a frequency of 5 Mega Samples per second (MSps), with a faster model, the LTC2386 produced by Analog Devices. The new ADCs are capable of matching the maximum speed of the ASIC's MUX of 10 MSps. This upgrade reduced the read time from 4 μs to 2 μs, maintaining a safe margin to account for potential delays. Additionally, we reduced the integration time from 1.4 μs to 100 ns, after experimental validation that this change does not compromise the detector's energy resolution. This is also expected from theoretical considerations, since the co-doped lanthanum bromide crystal has a fast decay time of 25 ns.

2.3. Optimization of materials

During Boron Neutron Capture Therapy (BNCT), the interaction of neutrons with surrounding materials can generate unwanted gamma rays, interfering with the useful signal that we wish to detect for dose monitoring purposes. The harsh measurement environment, characterized by a high neutron flux, makes it crucial to select materials that minimize these interactions and reduce background radiation. The primary challenge is the background radiation at 478 keV, as this is the energy at which the signal of interest from the boron neutron capture reactions occurs.

A significant source of background radiation at 478 keV is represented by the presence of boron in standard electronic circuit boards [24]. This represents a crucial problem because the boron in the boards undergoes neutron capture reactions, emitting gamma rays at the same energy as the signal of interest. Consequently, the boron content in the electronics can obscure the weak signal from the tumor, making it difficult to distinguish it from the background.

The substrate for Printed Circuit Boards (PCBs) is often realized using Flame Retardant 4 (FR4) material. FR4 is composed of glass fiber and epoxy resin, and it contains boron trioxide (B_2O_3), with boron content typically between 5% and 10% by weight. To resolve this issue, a new boron-free PCB substrate has been identified in the RO3003 Laminate, manufactured by Rogers Corporation. This unreinforced material does not contain glass fibers, thus lacking boron trioxide.

Experimental measurements were performed to compare the boron content in FR4 and RO3003 substrates by irradiating samples with neutrons. The resulting activation spectra showed a clear 478 keV peak in the FR4 sample, while no such peak was detected in the RO3003 sample [23]. Thus, all the PCBs in the BeNEdiCTE detector have been realized using the RO3003 substrate in place of the standard FR4 material.

Other possible boron-containing materials include the SiPMs and the ASICs, having ^{10}B in p-type semiconductor structures which use boron atoms as dopants. However, as detailed in [24], both their overall volume and their boron content are much lower with the respect to the printed circuit boards. Thus, it is reasonable to assume that the FR4 material in the PCBs had the larger contribution of ^{10}B atoms.

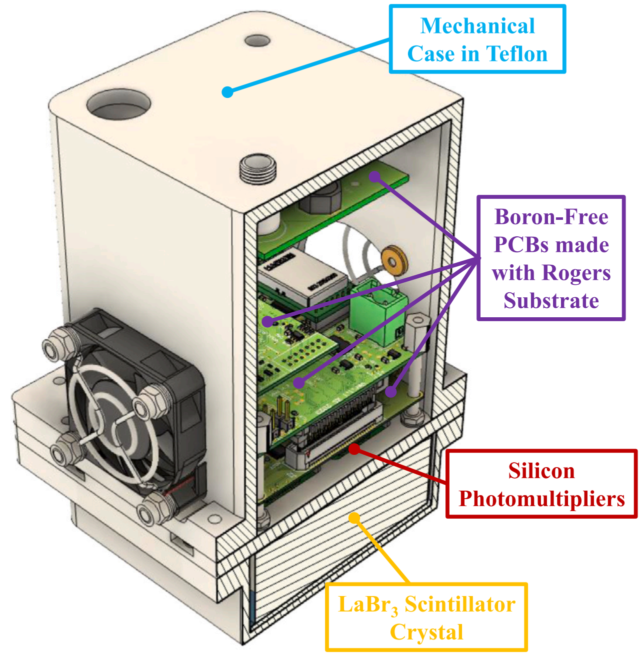

Fig. 1. Sectional view of the BeNEdiCTE detector, highlighting key upgrades in the use of new materials, including the boron-free PCBs with Rogers substrate and the new mechanical case in Teflon.

Another source of background radiation is represented by the presence of hydrogen, which induces gamma radiation at 2.2 MeV and lower energies due to neutron interactions. In the previous BeNEdiCTE detector, the 3D-printed PLA mechanical case contributed to this issue due to its hydrogen content. Additionally, the PLA case left the exposed electronics vulnerable to potential damage during operations.

To address these challenges, we developed a new case made of Teflon, a synthetic fluoropolymer composed exclusively of carbon and fluorine atoms. The new design provides improved mechanical stability, ensuring that the $LaBr_3$ crystal and SiPMs remain aligned throughout the measurements. Importantly, Teflon has negligible interaction with neutrons, minimizing the background radiation caused by neutron capture.

Fig. 1 shows a rendering sectional view of the BeNEdiCTE detector, displaying the main upgrades in terms of new materials.

2.4. New collimator design and artificial neural network

The SPECT module also includes a new collimator to ensure that the incoming radiation is effectively directed toward the BeNEdiCTE detector. The introduction of this new collimator is primarily driven by the need to reduce the overall volume of the SPECT module while preserving equivalent imaging performance. By minimizing the distances between the detector, collimator, and sample, the proposed design enables a more integrated and space-efficient SPECT module. This volume reduction is particularly relevant in the context of BNCT facilities, as it allows a significant decrease in the amount of required shielding materials.

The new collimator, shown in Fig. 2, is a single pinhole collimator made of lead, measuring 10 cm × 10 cm, with a thickness of 5 cm, and having a square aperture of 2 mm. The design parameters were selected to address the critical trade-off between sensitivity and spatial resolution, which is particularly challenging in a BNCT environment. Due to

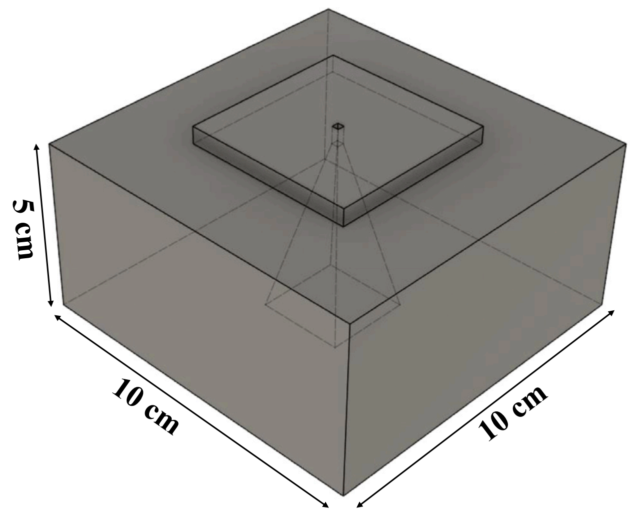

Fig. 2. View of the square pinhole collimator. The additional single channel collimator is also shown.

the relatively low yield of the 478 keV gamma rays emitted during the neutron capture reaction, maintaining an adequate geometric efficiency is crucial to ensure sufficient counting statistics. The 2 mm aperture was chosen as an optimal compromise, yielding a geometric efficiency of approximately 2.5×10^{-5} while ensuring a geometric resolution of 3 mm at the detector plane. The system's distances were geometrically constrained by the detector dimensions: positioning the pinhole 10 cm away from the detector surface and 20 cm away from the object plane provides a magnification factor of 0.5. This configuration effectively maps a 10 cm field-of-view (FoV) at the object onto the 5 cm FoV at the detector, perfectly matching the physical size of the crystal, with an acceptance angle of approximately 28° and a geometric resolution of 6 mm at the object plane.

Furthermore, the high energy of the 478 keV photons poses a significant challenge regarding septal penetration through the pinhole edges, which can severely degrade the spatial resolution. To mitigate this effect, an additional single-channel lead insert was attached to the pinhole aperture. This additional part of the collimator is made of lead, has a 2 mm square hole and 5 mm thickness. The impact of this design choice was quantitatively supported by an analytical model based on the Lambert–Beer law. By parameterizing the spatially varying thickness of the channel-edge region, the transmission of incident photons was computed using the linear attenuation coefficient of lead for 478 keV gamma rays. This theoretical workflow estimated a penetration-induced point spread function (PSF) of 3.6 mm. When this penetration component is convolved with the intrinsic detector resolution, the complete collimator assembly provides an overall estimated spatial resolution of 4.6 mm at the detector and 9.2 mm at the object.

An Artificial Neural Network (ANN), shown in Fig. 3, is used to reconstruct the positions of interaction of the gamma rays on the $LaBr_3$ monolithic crystal. The ANN is composed of an input layer comprising 64 neurons, corresponding to the signals coming from the 8 × 8 matrix of SiPMs. The input layer is followed by two hidden layers composed of 25 neurons each, using a hyperbolic-tangent activation function. The output layer consists of 3 neurons with linear activation function that predict the x, y, and z coordinates of interaction of the gamma rays on the scintillator crystal.

To optimize the network, the model was trained on an experimental 3D-labeled dataset acquired using a collimated ^{137}Cs source. Input data were preprocessed by filtering events within the 662 keV photopeak and normalizing the 64-channel signals. The training procedure was implemented in TensorFlow, utilizing the Adam optimizer and Mean Absolute Error (MAE) as the loss function. Furthermore,

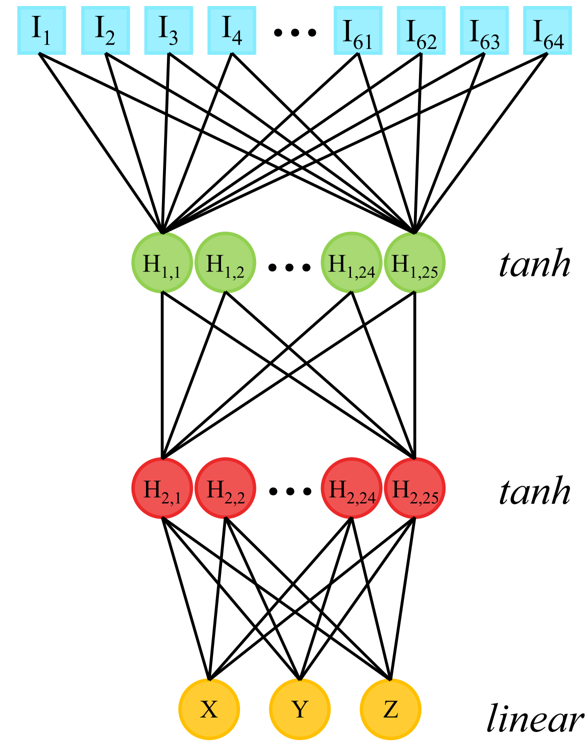

Fig. 3. Schematic description of the Artificial Neural Network used for position reconstruction.

the training workflow incorporated early-stopping callbacks to prevent overfitting on the validation set, and applied sample weights based on spatial voxelization to compensate for class imbalance. The final performance metrics were evaluated on dedicated test sets by extracting the Full Width at Half Maximum (FWHM) from the prediction error distributions.

The ANN is a new version of the one previously described in [25], incorporating DOI information. A comprehensive and exhaustive description of the experimental dataset acquisition, preprocessing pipeline, training architecture, and complete performance evaluation is detailed in [26].

2.5. Experimental configuration

We performed experimental measurements at the Prompt Gamma Neutron Activation Analysis facility of theTRIGA Mark II nuclear reactor at Laboratorio di Energia Nucleare Applicata (LENA), Pavia, Italy. The reactor was set at its maximal power of 250 kW. The thermal neutron fluence rate at the exit of the beam shaping assembly, where the sample was positioned, was approximately 3.14×10^6 n cm^{-2} s^{-1}. Different measurements have been performed to analyze the best shielding configuration, detect different boron concentrations, and obtain a 3D image of two borated vials.

2.5.1. Background analysis

For the measurements aiming at analyzing the background to find the best shielding configuration, we used two vials filled with distilled water as sample. Fig. 4 shows the experimental setup for these measurements in which the detector was not shielded.

The vials had a cylindrical shape, with an internal diameter of 6 mm and a height of 26 mm, leading to a volume of approximately 0.75 mL. The vials were positioned in front of the neutron beam on opposite vertices of a square support with a 1 cm side, resulting in a distance between their centers of $\sqrt{2}$ cm. The detector and collimator

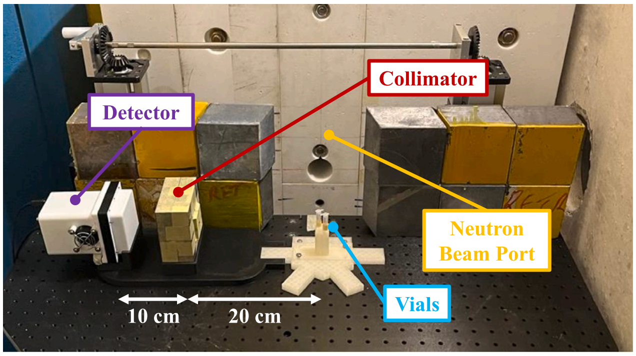

Fig. 4. Experimental configuration for the measurements aiming at analyzing the background. Distances between vials, collimator and detector are highlighted. The detector is not shielded.

were positioned perpendicularly to the direction of the neutron beam. The collimator was placed at a distance of 20 cm from the vial, while the detector was placed at a distance of 30 cm from the vial. All the measurements lasted for 5 min. Initially, two measurements were performed without any shielding material to analyze the effect of the material composing the electronics board. By changing all the PCBs of the BeNEdiCTE detector between the two measurements, any difference in the number of gamma rays recorded at 478 keV was analyzed. A first measurement was done using the FR4 PCBs, adopted in the previous prototype, followed by a second measurement using the PCBs made with RO3003.

Later, two measurements were performed to find the best shielding configuration. In both measurements, BeNEdiCTE detector was shielded from neutrons using cadmium foils. Cadmium was selected for its high cross section for thermal neutrons, which enabled effective absorption of thermal neutrons that could scatter into the irradiation room. Cadmium was chosen because, under the predominantly thermal neutron field available at the LENA beamline, cadmium foils provided sufficient neutron shielding for the purpose of these measurements while preserving a compact detector configuration. Moreover, the scattered thermal component to the detector is negligible considering the highly focalized neutron beam of the LENA beamline. In addition, the cadmium prompt gamma lines are far from the 478 keV energy region of interest and therefore did not prevent the identification of the boron signal. For the second measurement, an additional layer of shielding was added by using lead bricks. Lead was selected for its ability to shield photons that can be emitted by the interaction of neutrons with elements present in the room, but external to our system.

2.5.2. Different boron concentration

For the measurements aiming at detecting different boron concentrations, a single vial with a volume of 5 mL was used. Fig. 5 shows the experimental setup for these measurements.

The vial had a cylindrical shape, with an internal diameter of 14 mm and a height of 33 mm, and it was positioned in front of the neutron beam. The vial was filled with distilled water to acquire a background measurement, and then it was filled with solutions of boric acid with different concentrations ranging from 7371 ppm down to 250 ppm. The detector and collimator were positioned in the same positions as in the previous measurements. All the measurements lasted for 15 min, and the shielding configuration with both cadmium foils and lead bricks was used.

2.5.3. SPECT measurements

For the SPECT measurements, we used the same configuration of vials as in the measurements aiming at analyzing the background. The distances between vials, detector and collimator were the same. The

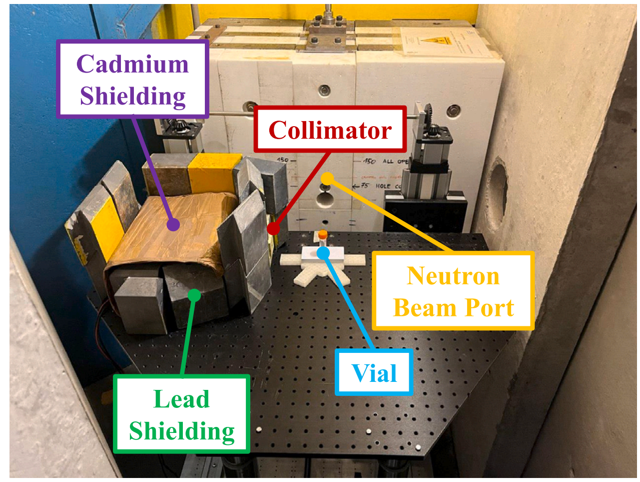

Fig. 5. Experimental configuration for the measurements aiming at monitoring different boron concentrations. The BeNEdiCTE detector is not visible due to the shielding. Cadmium and lead were used to shield neutrons and photons, respectively.

two vials were filled with a boric acid solution with a concentration of 7371 ppm. Also, background measurement were obtained by filling the two vials with distilled water. The measurement for each projection lasted for 15 min and the BeNEdiCTE detector was shielded using cadmium foils only. Due to space constraints within the irradiation room, the system was limited to performing only partial tomographic measurements. As a result, projection images were captured only at 0°, 60°, 120°, and 180°. The optimization of the SPECT measurement by introducing the DOI reconstruction in the detector is subject of a specific paper [26].

2.6. Spectrum processing

The acquired spectra were calibrated in energy by fitting known peaks, specifically the 478 keV from boron neutron capture and the 511 keV photopeak from annihilation photons. The peaks were fitted using Gaussian functions in Matlab, enabling the conversion of ADC values into corresponding energy levels. The detected counts were also normalized to the actual measurement time, ensuring that the data remained consistent and comparable across acquisitions with different durations. Furthermore, a correction to account for the dead time (DT) of the BeNEdiCTE detector were performed by multiplying the detected counts for a corrective factor. This factor was calculated as the ratio between the true input count rate (ICR) and the measured output count rate (OCR) at the detector. To compute ICR starting from the known OCR and DT, we used the equation $ICR = \frac{OCR}{1-(OCR \cdot DT)}$ [27].

To compute the number of counts per second (cps) in the 478 keV peak, the spectra were elaborated by subtracting the background using the SNIP algorithm [28]. Then, the two peaks at 478 keV and 511 keV were fitted simultaneously using two Gaussian functions in Matlab, and the cps are given by the area of the Gaussian functions.

2.7. Image processing

For each acquisition, events corresponding to the 478 keV peak were selected and processed by the ANN. Specifically, the selection was performed by fitting the 478 keV peak with a Gaussian function and retaining only the events falling within a $\pm 3\sigma$ energy window. The SiPM signals from these selected events were then fed into the neural network to predict the x, y, and z coordinates of interaction. Only those events with predicted coordinates $x, y \in [-25, 25]$ mm and $z \in [-10, 10]$ mm were kept, as this corresponds to the actual volume of

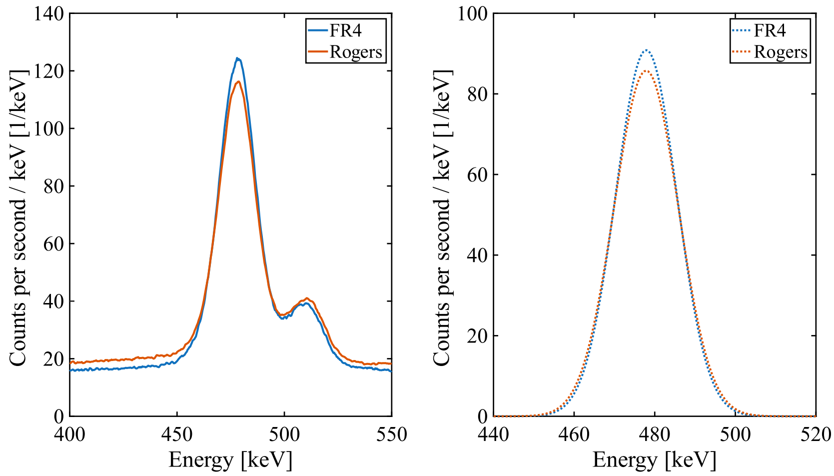

Fig. 6. (Left) Spectra acquired by the unshielded detector in the two measurements using FR4 and Rogers PCBs. The boron peak at 478 keV and the peak at 511 keV due to annihilation photons are visible. (Right) Gaussian fit of the peak at 478 after background subtraction, showing the higher number of events registered with FR4 PCBs.

the scintillator crystal. These events were organized into a 40 × 40 × 8 voxel grid with voxel dimensions of $1.25\ \mathrm{mm} \times 1.25\ \mathrm{mm} \times 2.5\ \mathrm{mm}$. For each projection, the background distribution was subtracted voxel by voxel from the boron distribution. The resulting difference dataset was corrected for DOI, yielding four DOI-adjusted 2D images that represent the final projections.

The 3D reconstruction from these four corrected projections was performed using STIR [29] with 30 iterations of the Maximum Likelihood Expectation Maximization algorithm. The number of iterations was selected as the optimal compromise between reconstruction accuracy and computational efficiency. The reconstructed volume was then subjected to an intensity-driven segmentation procedure. Initially, voxel intensities were rescaled to the interval $[0, 1]$. The binary mask generated is then applied to the original volume, zeroing out the background voxels while retaining the signal-containing regions. This segmentation step is crucial for minimizing residual background noise and isolating the activity associated with the vial, ensuring a more reliable assessment of the DOI correction.

3. Results

In this section, we present the results obtained from the experiments conducted with the single-unit SPECT module described in Section 2. The results will focus on the effectiveness of different shielding configurations, the detection of boron at varying concentrations, and the generation of 3D images of borated vials.

3.1. Background analysis

The first measurements performed with vials filled with water and without any shielding revealed a very high peak around 478 keV. Being the vials completely free of boron, this peak could only be due to background contributions.

An important aspect is represented by the printed circuit boards (PCBs), which contains boron if realized with the standard FR4 substrate. Fig. 6 shows the results of the measurements performed to analyze the difference between the PCBs made with FR4 and the PCBs made with the boron-free Rogers RO3003 substrate.

A very high peak around 478 keV is present in both measurements, also because of the absence of any shielding material. Without cadmium shielding, a significantly higher flux of scattered thermal neutrons can easily reach the detector and interact with its internal components. Consequently, the residual peak around 478 keV is largely attributed to the neutron-induced background generated directly inside the detectors, specifically, from the activation of the scintillator crystal, given the non-negligible thermal neutron capture cross-sections of both Lanthanum and Bromine isotopes, as better discussed in Section 4. However, a noticeable difference can be observed in the 478 keV peak between the two measurements. This difference can only be attributed to the contributions of the PCBs, as they are the only element which was changed in the experimental setup between the two measurements. The 478 keV peak has an area of 1728 ± 12 cps in the measurement with FR4 PCBs, and an area of 1518 ± 11 cps in the measurement with Rogers PCBs. Thus, the contribution from boron present in the FR4 material constituting PCBs can be estimated in 210 ± 16 cps.

The second set of measurements, aiming at evaluating different strategies to reduce the background, consisted of comparing two possible shielding configurations. Fig. 7 shows the comparison between the spectrum acquired using only cadmium shielding and the one acquired using cadmium and lead shielding. It can be seen that the peak around 478 keV is drastically reduced in both measurements, compared to the one obtained in the previous measurements. However, a small difference can be seen in the peak around 478 keV between the two measurements, meaning that also lead shielding is needed to prevent a small but present contribution of photons generated by the interaction of neutrons with surrounding materials in the environment.

The peak around 478 keV has an area of 38.2 ± 7.4 cps in the measurement with cadmium shielding only, and an area of 24.5 ± 10.0 cps in the measurement with cadmium and lead shielding. Thus, the contribution from gamma rays generated by the interaction of neutrons with surrounding materials can be estimated in 13.7 ± 12.4 cps.

3.2. Different boron concentration

Having found a good shielding configuration, we performed a series of measurements to detect different boron concentrations. In addition to the background measurement performed with a vial filled of distilled water, five other measurements have been performed. In these measurements, the vial has been filled with a boric acid solution with concentrations of 7371 ppm, 3685 ppm, 965 ppm, 500 ppm, and 250 ppm. Fig. 8 shows the results of these measurements.

The quantitative results of the fitting procedure of the peak at 478 keV are shown in Table 1.

The third column of the table has been obtained by subtracting the number of events detected in the measurement with water (i.e., 0 ppm) to the number of events registered in each measurement. The reported uncertainties represent the standard error of the peak area parameter extracted directly by the Gaussian fitting algorithm. Indeed, because the

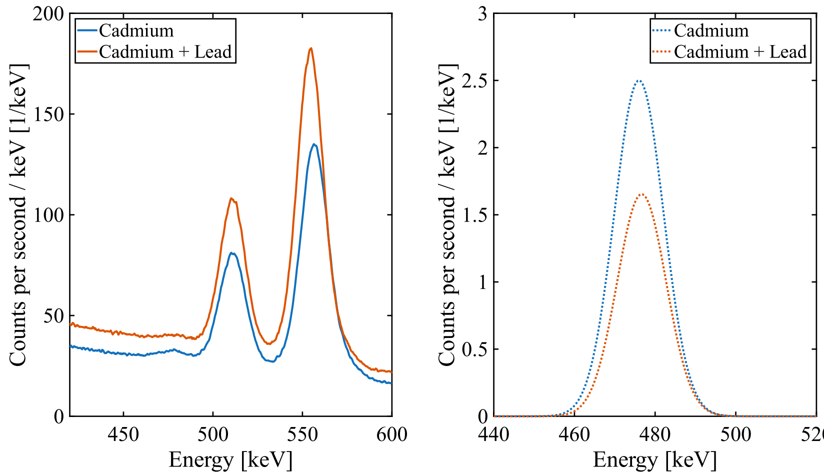

Fig. 7. (Left) Spectra acquired by the detector in the two measurements using different shielding. The peaks at 478 keV, 511 keV and 559 keV, due to boron background, annihilation photons, and cadmium neutron capture, are visible. (Right) Gaussian fit of the peak at 478 keV, showing the higher number of events registered when lead was not used.

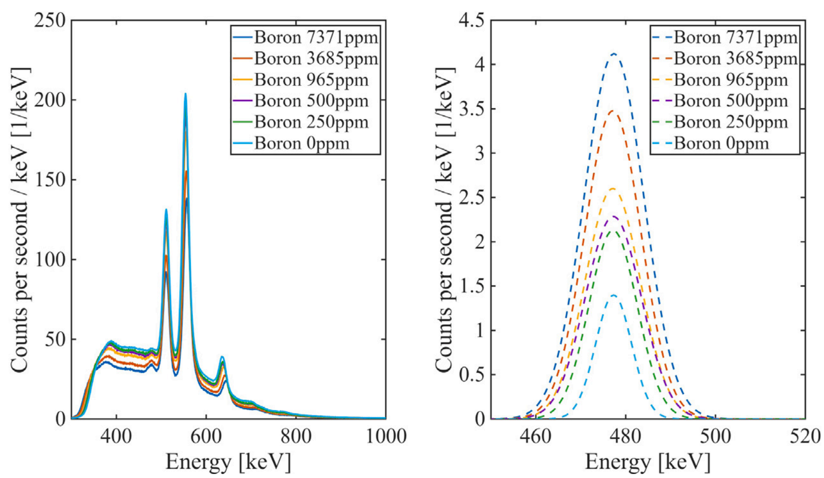

Fig. 8. (Left) Spectra acquired by the detector in the measurements with different boron concentrations. The peaks at 478 keV and 511 keV due to boron and annihilation photons are visible. Also the peaks at 559 keV and 651 keV due to cadmium neutron capture are visible. (Right) Gaussian fit of the peak at 478 keV, showing proportionality between boron concentration and number of events registered at 478 keV.

Table 1
Results of the fitting procedure in the measurements performed with different boron concentration.

Boron concentration [ppm]	Cps at 478 keV	Net cps at 478 keV
7371	68.71 ± 7.27	54.65 ± 8.92
3685	54.40 ± 7.08	40.33 ± 8.76
965	41.06 ± 7.35	26.99 ± 8.98
500	35.48 ± 7.71	21.41 ± 9.28
250	28.47 ± 7.15	14.41 ± 8.82
0	14.07 ± 5.16	–

478 keV peak sits on top of a significant background continuum, the dominant source of uncertainty is the mathematical limitation of the fitting algorithm in isolating the net signal. This results in a conservative and nearly constant error bound across the measurements. Finally, the uncertainties on the net count rates were propagated by summing in quadrature the fitting errors of the respective gross measurement and the background (0 ppm) measurement.

Fig. 9 illustrates the dependence of the net count rate under the 478 keV peak on the boron concentration. The data exhibits a linear behavior at low concentrations, represented by the dashed line. However, at higher concentrations, a departure from linearity is observed. This saturation effect at higher concentrations (well above 1000 ppm) is physically driven by neutron self-shielding [30], as also confirmed by our FLUKA Monte Carlo simulations. At high boron concentrations, the high capture cross-section of ^{10}B causes the outer layers of the sample to absorb a large fraction of the incident neutrons, shielding the inner volume. This prevents the neutron flux from reacting uniformly with all the boron present, effectively reducing the slope of the curve. At lower concentrations (e.g., 965 ppm), a deviation from the expected linearity is not attributed to self-shielding, but rather to an analytical artifact. As previously discussed, the small peak area on top of a significant background continuum causes the Gaussian fitting algorithm to struggle in accurately isolating the net signal, leading to the substantial fitting uncertainties presented earlier.

3.3. SPECT measurements

SPECT measurements involved performing eight acquisition at four different angles. For each angle, two measurement were performed. A first background measurement was acquired using vials filled with water, and a second measurement was acquired with vials filled with

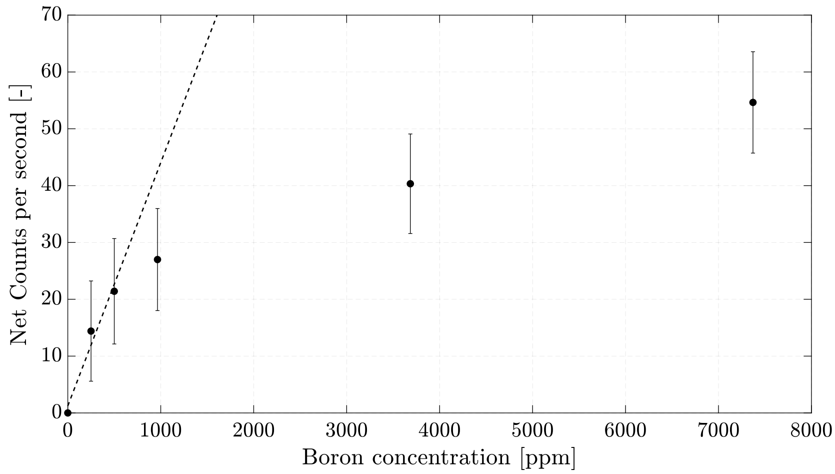

Fig. 9. Net counts per second at 478 keV versus boron concentration. A trend line for low concentrations is plotted to show the dependence of the net count rate under the 478 keV peak on the boron concentration. At high concentrations, the self-shielding phenomenon causes a saturation effect.

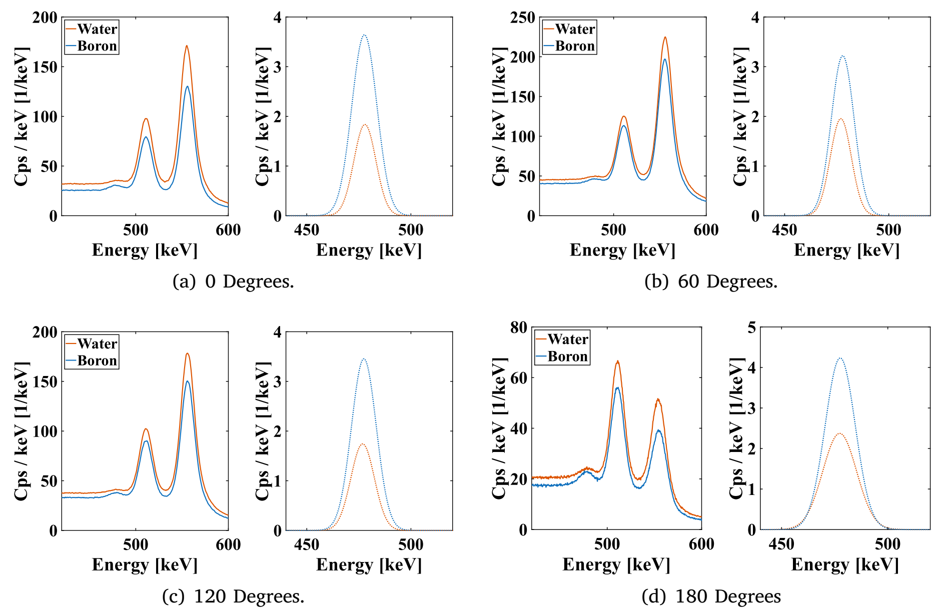

Fig. 10. For each of the four angles, the plot on the left shows the spectra acquired by the detector. The plot on the right shows the Gaussian fit of the peak at 478 keV, highlighting a higher number of events during the measurements with boric acid.

boric acid. The energy spectra of the eight measurements are shown in Fig. 10.

The results of the fitting procedure of the peak at 478 keV are shown in Table 2.

The lateral and top view of the vials reconstructed in 3D is shown in Fig. 11.

Table 2
Results of the fitting procedure in the SPECT measurements.

Angle	Sample	Cps at 478 keV	Net cps at 478 keV
0	Water	24.31 ± 6.10	30.90 ± 7.94
	Boron	55.21 ± 5.09	
60	Water	24.73 ± 8.73	19.49 ± 11.65
	Boron	44.22 ± 7.72	
120	Water	24.65 ± 6.35	26.94 ± 8.76
	Boron	51.59 ± 6.03	
180	Water	47.44 ± 5.21	27.96 ± 6.58
	Boron	75.41 ± 4.02	

4. Discussion

The experimental results presented in this work provide a comprehensive interpretation of the origin of the background at 478 keV during measurements aiming at prompt gamma detection in BNCT environments. In particular, the measurements performed at the LENA reactor allowed us to understand the different contributions to the 478 keV background and to assess the effectiveness of both material optimization and shielding configurations.

A first key outcome of this study is the clear identification of two distinct sources of background gamma rays around 478 keV:

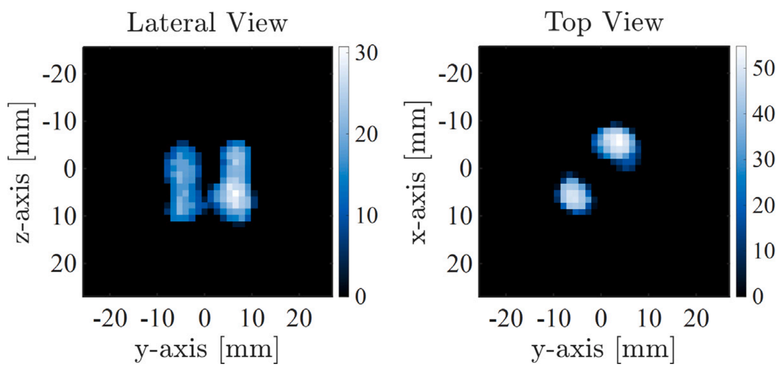

Fig. 11. Lateral and top view of the reconstructed 3D volumes, displaying the two vials used as sample. The 3D reconstruction was performed starting from four 2D projections, which were previously corrected background via a pixel-by-pixel subtraction of a boron-free water measurement.

1. Gamma rays generated internally within the system: these gamma rays result from the interaction of neutrons with components of the SPECT module. These interactions can produce gamma rays around 478 keV if boron, or other materials emitting around the energy of interest, are present in some elements of the SPECT module. To minimize this internal background, effective neutron shielding is required. Materials such as cadmium are commonly used to absorb neutrons and prevent such interactions.
2. Gamma rays generated externally in the room: these gamma rays are produced by the interaction of neutrons with surrounding materials in the environment, including the walls and other objects in the room. If boron or other materials emitting around the energy of interest are present in the room, the result is the creation of 478 keV gamma rays that can be measured by the detection system. To mitigate this external background, gamma-ray shielding is essential, typically achieved using lead or other dense materials capable of attenuating this type of radiation.

Concerning gamma rays generated internally to the system, the activation of the $LaBr_3$ scintillator crystal can play a role. Indeed, the isotope ^{139}La can undergo a neutron capture reaction, producing ^{140}La. This isotope is unstable and has among its decay products a 487 keV gamma ray. Despite the excellent energy resolution of the BeNEdiCTE detector, gamma rays at 487 keV cannot be resolved from gamma rays at 478 keV. Thus, the activation of the scintillator crystal represents a source of background radiation at the energy of interest. Another important source of background is represented by the printed circuit boards (PCBs), as will be discussed more in detail.

Concerning gamma rays generated externally to the system, the presence of boron in the walls of the facility can be a source of background radiation at the energy of interest. Despite the presence of boron is not known in the materials used to build LENA facility where the measurements have been performed, we can deduce from the measurements that traces of boron could be present. Indeed, a detectable peak at 478 keV has been measured also without boron in the irradiated samples. In general, boron is often used as a shielding material in the walls of facilities designed for neutron irradiation, due to its very high neutron capture cross section of 3848 barns. Therefore, 478 keV signal from the environment will always have to be considered and appropriate shielding should be arranged to reduce its contribution.

The measurements performed without any shielding highlight the combined effect of these two contributions. In this configuration, a very intense peak around 478 keV is observed even in the absence of boron in the irradiated vials, confirming that the background is dominated by neutron-induced interactions rather than by the sample itself.

Despite the presence of common background sources, the comparison between FR4 and Rogers RO3003 PCBs clearly highlights the influence of electronics board materials on the background. The significantly higher count rate measured with FR4 PCBs directly reflects the presence of boron in the FR4 substrate, whereas the reduced peak observed with Rogers PCBs demonstrates the effectiveness of boron-free materials in suppressing part of the internally generated background. The difference of 210 cps between the FR4 and Rogers boards may result not too large relative to the 478 keV peak intensity. Indeed, in this measurements without shielding and with a thermal neutron beam, the external background and the activation of other materials inside the system, such as the scintillator crystal, also contribute to the background around 478 keV. However, the situation is very different in facilities with epithermal neutron beam and measurements with proper shielding, as will be highlighted below.

The introduction of cadmium shielding represents a crucial step in background mitigation in a facility with a thermal neutron beam. Cadmium efficiently absorbs thermal neutrons, thereby preventing their interaction with the detector components and electronics. The experimental results clearly show that, when cadmium shielding is applied, the high peak at 478 keV peak previously observed disappears. This indicates that the cadmium enclosure is effective and, under this configuration, thermal neutrons no longer interact with the system itself.

These results indicate that, under the specific irradiation conditions of the LENA facility, the internally generated background at 478 keV can be effectively suppressed by means of cadmium shielding. Indeed, since the neutron beam available at LENA is predominantly thermal, cadmium absorption is highly efficient in preventing neutrons from interacting with the detector components. However, the situation is different in a clinical BNCT environment, where epithermal neutron beams are employed to achieve sufficient penetration depth before thermalization in tissue. While several shielding strategies can be adopted to attenuate epithermal neutrons, it is considerably more challenging to completely suppress their interaction with the detector system. Consequently, a fraction of neutrons is expected to reach the detector and surrounding materials, where they may thermalize and induce neutron capture reactions [22]. In this scenario, the presence of boron within the detector components becomes critical, as it would lead to the generation of undesired 478 keV gamma rays that are indistinguishable from the signal of interest. When an epithermal neutron beam is used, and the external background is shielded properly by means of lead bricks, the dominant background contribution is expected to come from the boron inside the PCBs. Indeed, the elements inside the scintillator crystal have a lower cross-section for epithermal neutrons, and the external background can be shielded more easily. For this reason, the use of boron-free materials, such as Rogers RO3003 PCBs, remains a fundamental design requirement for BNCT prompt gamma detection systems intended for clinical deployment.

Despite the effectiveness of cadmium shielding at LENA facility, a non-zero background at 478 keV is still observed when cadmium shielding alone is used. The persistence of this residual peak points to an external origin, namely gamma rays produced outside the system and entering the detector volume. The comparison between measurements performed with cadmium-only shielding and those performed with the additional lead shielding provides a clear interpretation. The further reduction of the 478 keV peak achieved by adding lead demonstrates that a fraction of the background is due to photons generated externally, most likely from neutron interactions with boron-containing materials in the room.

Taken together, these results show that, at the LENA facility, both neutron and photon shielding are essential. Cadmium is required to suppress neutron interactions within the detector system, while lead is necessary to attenuate gamma rays produced in the surrounding environment.

The measurements performed with increasing boron concentrations demonstrate a clear relationship between the intensity of the 478 keV peak and the amount of^{10}B present in the sample. This confirms the capability of the system to quantitatively monitor boron concentration through prompt gamma detection. This proportionality indicates that, once background contributions are properly mitigated, the detector response is primarily driven by the neutron capture rate in boron and can therefore be exploited for concentration monitoring. Furthermore, the system's confirms its excellent energy resolution around 4% at 478 keV, clearly distinguishing this peak from the adjacent 511 keV peak from annihilation photons. This energy resolution outperforms recent prototypes based on Electron-Tracking Compton Cameras (ETCC) based on GAGG, thus providing a superior capability to discriminate the useful signal [31].

From a sensitivity perspective, the system was able to reliably detect boron concentrations down to 250 ppm of^{10}B in a volume of 5 mL. This is a very significant improvement with respect to the previous measurements with the BeNEdiCTE SPECT module. Indeed, when coupling the detector with the collimator, the system could never detect concentrations below 1000 ppm. Furthermore, the thermal neutron flux used at LENA during measurements was about 3.14×10^6 n cm^{-2} s^{-1}, more than two orders of magnitude lower than the flux commonly employed in clinical BNCT facilities, which is of the order of 1×10^9 n cm^{-2} s^{-1}. Based purely on the linear scaling of the reaction rate, the theoretical sensitivity at clinical fluxes would approach a few ppm, which is well within the clinically relevant range. However, this extrapolation represents an ideal behavior. In a clinical environment, also the scaling of background radiation must be accounted for, as it will inevitably affect the signal-to-noise ratio (SNR). Furthermore, the intense flux will dramatically increase the overall event rate, introducing pile-up effects and detector dead time. Nevertheless, the recent enhancements in the system's count-rate capability were specifically developed to address these high-rate challenges. In this view, the recent increase in count-rate capability is promising, but experimental measurements are still needed to verify the behavior of the detector in those conditions.

Finally, SPECT measurements revealed the system capability to detect the boron signal at all angles. While numerous recent studies have relied primarily on Monte Carlo simulations to assess the feasibility of BNCT-SPECT or Compton Camera systems [12,32], this work provides direct experimental validation of the detector's performance in a realistic reactor environment. Compared to the previous campaign [19], even at the maximal reactor power of 250 kW, the spectra at 60° and 120° show a clear 478 keV boron peak. Thus, there is no more need for further processing, such as a reconstruction of the spectra based on the coordinates predicted by the ANN, to extract signal over the background. This improvement can be attributed to the reduction of the detector's dead time, which mitigates pile-up between events at high rates and provides higher count-rate capability, and to the higher local signal-to-noise ratio (SNR) provided by the new collimator.

The system was also able to reconstructed a 3D image in which the two vials are clearly distinguishable and well separated. Both the dimensions of the vials and their relative position in the reconstructed image are coherent with the experimental setup. This confirms the system's capability to achieve a spatial resolution better than 1 cm.

5. Conclusions

We proposed a single-unit SPECT module based on a new version of the BeNEdiCTE gamma-ray detector for dose monitoring in Boron Neutron Capture Therapy (BNCT). The detector is based on a monolithic lanthanum bromide scintillator crystal and it is coupled with a custom-designed pinhole collimator made of lead.

With this system, we performed experimental measurements with a nuclear reactor at LENA, Pavia. The system has shown the capability to detect boron concentrations down to 250 ppm in volumes of 5 mL with a neutron flux of 3.14×10^6 n cm^{-2} s^{-1}. The detector's energy resolution, approximately 4% at 478 keV, allows the boron peak to be clearly distinguished from the 511 keV annihilation peaks, making the system highly accurate for monitoring boron distribution.

A crucial aspect that emerged from this work is the importance of optimizing materials to reduce background interference. Measurements have shown that the materials used in the construction of printed circuit boards have a significant impact on radiation background, with a notable difference between standard FR4 PCBs, which contain boron, and those made with boron-free RO3003 material. With regard to shielding configurations, the results confirm the effectiveness of cadmium shielding in reducing the thermal neutron background. However, although cadmium shielding is sufficient to reduce the background generated by the interaction of neutrons with the system components, the use of additional shielding, such as lead, is necessary to attenuate the photons generated by the interaction of neutrons with surrounding materials.

Furthermore, measurements taken with increasing boron concentrations confirmed a clear correlation between the intensity of the peak at 478 keV and the concentration of^{10}B in the sample, highlighting the system's ability to quantitatively monitor boron concentration through gamma ray detection. This result suggests that, once background contributions are properly managed, the system can be used effectively for real-time monitoring of boron concentrations, making it a valuable tool for clinical BNCT. Finally, tomographic measurements showed that the system is capable to acquire accurate three-dimensional images and achieve a spatial resolution of less than 1 cm. These results are promising for future clinical applications, where it will be necessary to monitor boron distribution in real time during treatment.

As future steps, measurements with neutron fluxes on the order of magnitude of those used in BNCT should be performed to evaluate the detector's capability to handle high rates of events. Also, measurements using samples with boron concentrations at which self-absorption is negligible would make it possible to further confirm the linearity of the system's response.

CRediT authorship contribution statement

F. Ghisio: Writing – original draft, Software, Methodology, Data curation, Conceptualization. **T. Ferri:** Software, Investigation, Data curation. **M. Pandocchi:** Software, Investigation, Data curation. **M. Carminati:** Writing – review & editing, Project administration, Funding acquisition. **C. Fiorini:** Writing – review & editing, Supervision, Project administration. **G. Mocerino:** Software, Investigation, Data curation. **L. Grisoni:** Software, Investigation, Data curation. **D. Mazzucconi:** Supervision, Project administration. **D. Ramos:** Software, Data curation. **G. Iaselli:** Supervision, Project administration. **G. Pugliese:** Supervision, Project administration. **V. Pascali:** Software, Data curation. **N. Protti:** Supervision, Project administration. **G. Borghi:** Writing – review & editing, Supervision, Project administration, Funding acquisition.

Declaration of competing interest

The authors declare that they have no known competing financial interests or personal relationships that could have appeared to influence the work reported in this paper.

Data availability

The data generated and analyzed during the current study can be provided on reasonable request.

References

[1] J. Ferlay, M. Ervik, F. Lam, M. Laversanne, M. Colombet, L. Mery, M. Piñeros, A. Znaor, I. Soerjomataram, F. Bray, Global cancer observatory: Cancer today, 2024, URL https://gco.iarc.who.int/today.

[2] M. Durante, J.S. Loeffler, Charged particles in radiation oncology, Nat. Rev. Clin. Oncol. 7 (1) (2010) 37–43.

[3] W.A.G. Sauerwein, K. Igawa, J. Herault, P. Fossati, S. Altieri, R.L. Moss, A. Wittig, Hadron therapy in radiation oncology and why BNCT is a paradigm shift, Health Technol. 14 (5) (2024) 995–1000.

[4] D. Skwierawska, J.A. López-Valverde, M. Balcerzyk, A. Leal, Clinical viability of boron neutron capture therapy for personalized radiation treatment, Cancers 14 (12) (2022) 2865.

[5] W. Sauerwein, A. Wittig, R. Moss, Y. Nakagawa, Neutron Capture Therapy. Principles and Applications, Springer, 2012.

[6] D.N. Slatkin, A history of boron neutron capture therapy of brain tumours. Postulation of a brain radiation dose tolerance limit, Brain: A J. Neurol. 114 (Pt 4) (1991) 1609–1629.

[7] M. Suzuki, Y. Sakurai, S. Hagiwara, S. Masunaga, Y. Kinashi, K. Nagata, A. Maruhashi, M. Kudo, K. Ono, First attempt of boron neutron capture therapy (BNCT) for hepatocellular carcinoma, Jpn. J. Clin. Oncol. 37 (5) (2007) 376–381.

[8] M. Suzuki, Boron neutron capture therapy (BNCT): A unique role in radiotherapy with a view to entering the accelerator-based BNCT era, Int. J. Clin. Oncol. 25 (2020).

[9] International Society for Neutron Capture Therapy, Accelerator-based BNCT projects, 2025, URL https://isnct.net/bnct-boron-neutron-capture-therapy/accelerator-based-bnct-projects-2021/.

[10] Y. Imahori, S. Ueda, Y. Ohmori, K. Sakae, T. Kusuki, T. Kobayashi, M. Takagaki, K. Ono, T. Ido, R. Fujii, Positron emission tomography-based boron neutron capture therapy using boronophenylalanine for high-grade gliomas: Part I, Clin. Cancer Res. 4 (8) (1998) 1825–1832.

[11] Z. Hou, C. Geng, X. Tang, F. Tian, S. Zhao, J. Qi, D. Shu, C. Gong, Boron concentration prediction from Compton camera image for boron neutron capture therapy based on generative adversarial network, Appl. Radiat. Isot. 186 (2022) 110302.

[12] K. Nutter, T. Price, T. Kokalova, S. Green, B. Phoenix, A feasibility study using an array of LaBr3(Ce) scintillation detectors as a Compton camera for prompt Gamma imaging during BNCT, Front. Phys. 12 (2024).

[13] P. Torres-Sánchez, J. Lerendegui-Marco, J. Balibrea-Correa, V. Babiano-Suárez, B. Gameiro, I. Ladarescu, P. Álvarez-Rodríguez, J.-M. Daugas, U. Koester, C. Michelagnoli, M. Pedrosa-Rivera, I. Porras, M.J. Ruiz-Magaña, C. Ruiz-Ruiz, C. Domingo-Pardo, The I-TED compton camera array for real-time boron imaging and determination during treatments in boron neutron capture therapy, Appl. Radiat. Isot. 217 (2025) 111649.

[14] T. Kobayashi, Y. Sakurai, M. Ishikawa, A noninvasive dose estimation system for clinical BNCT based on PG-SPECT—Conceptual study and fundamental experiments using HPGe and CdTe semiconductor detectors, Med. Phys. 27 (9) (2000) 2124–2132.

[15] D.M. Minsky, A.A. Valda, A.J. Kreiner, S. Green, C. Wojnecki, Z. Ghani, First tomographic image of neutron capture rate in a BNCT facility, Appl. Radiat. Isot. 69 (12) (2011) 1858–1861.

[16] B. Hales, T. Katabuchi, M. Igashira, K. Terada, N. Hayashizaki, T. Kobayashi, Predicted performance of a PG-SPECT system using CZT primary detectors and secondary Compton-suppression anti-coincidence detectors under near-clinical settings for boron neutron capture therapy, Nucl. Instrum. Methods Phys. Res. Sect. A: Accel. Spectrometers, Detect. Assoc. Equip. 875 (2017) 51–56.

[17] I. Murata, S. Kusaka, K. Minami, N. Saraue, S. Tamaki, I. Kato, F. Sato, Design of SPECT for BNCT to measure local boron dose with GAGG scintillator, Appl. Radiat. Isot. 181 (2022) 110056.

[18] A. Caracciolo, T. Ferri, G. Borghi, M. Carminati, N. Protti, S. Altieri, C. Fiorini, A compact scintillator-based detector with collimator and shielding for dose monitoring in boron neutron capture therapy, Phys. Imaging Radiat. Oncol. 29 (2024) 100556.

[19] T. Ferri, A. Caracciolo, F. Ghisio, M. Piroddi, M. Pandocchi, C. Fiorini, M. Carminati, V. Pascali, N. Protti, D. Mazzucconi, L. Grisoni, D. Ramos, N. Ferrara, K. Thielemans, G. Borghi, Design and validation of a SPECT prototype for treatment monitoring in BNCT and first experimental tomographic results, IEEE Trans. Radiat. Plasma Med. Sci. (2025) 1–1.

[20] A. Gola, F. Acerbi, M. Capasso, M. Marcante, A. Mazzi, G. Paternoster, C. Piemonte, V. Regazzoni, N. Zorzi, NUV-sensitive silicon photomultiplier technologies developed at Fondazione Bruno Kessler, Sensors 19 (2) (2019) 308.

[21] L. Buonanno, D.D. Vita, M. Carminati, C. Fiorini, GAMMA: A 16-channel spectroscopic ASIC for SiPMs readout with 84-dB dynamic range, IEEE Trans. Nucl. Sci. 68 (10) (2021) 2559–2572.

[22] A. Caracciolo, D. Mazzucconi, T. Ferri, L. Grisoni, F. Ghisio, M. Piroddi, G. Borghi, M. Carminati, S. Agosteo, K. Tsuchida, T. Nishitani, Y. Ichikawa, A. Uritani, S. Altieri, N. Protti, C. Fiorini, Prompt Gamma-ray imaging in realistic background conditions of a boron neutron capture therapy facility, Sci. Rep. 15 (1) (2025) 18626.

[23] F. Ghisio, T. Ferri, A. Caracciolo, S. Agosteo, S. Altieri, C. Fiorini, M. Carminati, L. Grisoni, G. Iaselli, Y. Ichikawa, D. Mazzucconi, N. Protti, L. Santini, K. Tsuchida, G. Borghi, Towards clinical integration of a SPECT detection module for BNCT dose monitoring, EPJ Web Conf. 338 (2025) 09001.

[24] G. Colombo, A. Caracciolo, D. Mazzucconi, G. Borghi, M. Carminati, N. Protti, S. Altieri, S. Agosteo, C. Fiorini, Study of the thermal neutron activation of a Gamma-ray detector for BNCT dose monitoring, J. Instrum. 19 (05) (2024) P05047.

[25] T. Ferri, F. Rosellini, A. Caracciolo, G. Borghi, M. Carminati, F. Camera, A. Giaz, C. Fiorini, Gamma-ray position-of-interaction estimation in a thick monolithic $LaBr_3$ detector using artificial neural networks, IEEE Trans. Radiat. Plasma Med. Sci. (2025).

[26] T. Ferri, F. Ghisio, M. Carminati, C. Fiorini, M. Pandocchi, L. Pompigna, D. Mazzucconi, G. Mocerino, N. Protti, G. Borghi, Development of an Optimized SPECT Module for BNCT Applications with Novel Pinhole Collimator and DOI Estimation with ANN, IEEE Trans. Radiat. Plasma Med. Sci. (2026).

[27] G.F. Knoll, Radiation Detection and Measurement, fourth ed., Wiley, Hoboken, NJ, 2010.

[28] C.G. Ryan, E. Clayton, W.L. Griffin, S.H. Sie, D.R. Cousens, SNIP, a statistics-sensitive background treatment for the quantitative analysis of PIXE spectra in geoscience applications, Nucl. Instrum. Methods Phys. Res. Sect. B: Beam Interactions Mater. Atoms 34 (3) (1988) 396–402.

[29] K. Thielemans, C. Tsoumpas, S. Mustafovic, T. Beisel, P. Aguiar, N. Dikaios, M.W. Jacobson, STIR: Software for tomographic image reconstruction release 2, Phys. Med. Biol. 57 (4) (2012) 867.

[30] R.F. Fleming, Neutron self-shielding factors for simple geometrics, Int. J. Appl. Radiat. Isot. 33 (11) (1982) 1263–1268.

[31] T. Mizumoto, S. Komura, A. Takada, Y. Sakurai, T. Tanimori, Quantitative imaging of 478-keV prompt Gamma rays from boron neutron capture reactions, Sci. Rep. 15 (1) (2025) 29310.

[32] J. Fan, Q. Jiang, Y. Hu, Z. Han, Y. Dai, Y. Liu, K. Liu, T. Atsushi, M. Yan, S. Wang, Design of a PG-SPECT for boron concentration monitoring in BNCT at XJTU, Nucl. Eng. Technol. 57 (7) (2025) 103499.